Structural basis for pH dependent monomer-dimer transition of 3,4-dihydroxy 2-butanone-4-phosphate synthase domain from *M. tuberculosis*

Mirage Singh, Pankaj Kumar, Subramanian Karthikeyan*

Division of Protein Science and Engineering
Institute of Microbial Technology
Council of Scientific and Industrial Research (CSIR)
Sector 39-A, Chandigarh – 160 036, India

Running title: Crystal structure of DHBPS domain from *M. tuberculosis*

Corresponding author:

S. Karthikeyan, Ph. D.
Institute of Microbial Technology (CSIR)
Sector 39-A, Chandigarh – 160 036, India.
Fax: +91-172-2690585
Email: skarthik@imtech.res.in

ABSTRACT

3,4-dihydroxy 2-butanone 4-phosphate synthase (DHBPS) and GTP cyclohydrolase-II (GTPCH-II) are the two initial enzymes involved in riboflavin biosynthesis pathway, which has been shown to be essential for the pathogens. In *Mycobacterium tuberculosis* (*Mtb*), the *ribA2* gene (Rv1415) encodes for the bi-functional enzyme with DHBPS and GTPCH-II domains at N- and C-termini, respectively. We have determined three crystal structures of *Mtb*-DHBPS domain in complex with phosphate and glycerol at pH 6.0, with sulphate at pH 4.0 and with zinc and sulphate at pH 4.0 at 1.8 Å, 2.06 Å and 2.06 Å resolution respectively. The hydrodynamic volume and enzyme activity studies revealed that the *Mtb*-DHBPS domain forms a functional homo-dimer between the pH 6.0–9.0, however, at pH 5.0 and below, it forms a stable inactive monomer in solution. Furthermore, the functional activity of *Mtb*-DHBPS and its dimeric state could be restored by increasing the pH between 6.0 to 9.0. The comparison of crystal structures determined at different pH revealed that the overall three-dimensional structure of *Mtb*-DHBPS monomer remains the same. However, the length of the α6-helix at pH 6.0 has increased from 15 Å to 22 Å in pH 4.0 by increasing the number of amino acids contributing to the α6-helix from 11 to 15, achieving a higher structural stability at pH 4.0. Taken together our experiments strongly suggest that the *Mtb*-DHBPS domain can transit between inactive monomer to active dimer depending upon its pH values, both in solution as well in crystal structure.

Keywords: Riboflavin, FMN/FAD, antibacterial, drug target, vitaminB2

1. Introduction

The emergence of multiple drug resistance in pathogenic bacteria has posed a serious threat to human health around the world. One such example is the increasing multiple drug resistance in *M. tuberculosis (Mtb)*, (Russell et. al., 2010) a major human pathogen responsible for the death of millions of people every year across the globe. With the emergence of drug resistance in *Mtb* there is significant increase in mortality of tuberculosis (TB) patients. According to world health organization, drug resistant TB claimed 1.5 million lives across the globe in 2008 (WHO report, 2010). This situation demands the formulation of new antibiotics as well as the identification of new targets that could be exploited as novel anti-bacterial drug targets. The enzymes involved in riboflavin biosynthesis pathway are attractive drug targets as this pathway has been shown to be essential for the micro-organisms including *Mtb*, but absent in humans. (Philipp et. al., 1996; Cole et. al., 2001; Gerdes et. al., 2002; Sassetti et. al., 2003).

In riboflavin biosynthesis pathway, 3,4-dihydroxy-2-butanone-4-phosphate synthase (DHBPS) catalyzes the conversion of D-ribulose-5-phosphate to L-3,4-dihydroxy-2-butanone-4-phosphate (DHBP) and formate (Fig. 1) (Volk and Bacher, 1990; Volk and Bacher 1991; Richter et. al., 1992). From another branch of this pathway, Guanosine-5'-triphosphate (GTP) cyclohydrolase-II (GTPCH-II) catalyzes the conversion of GTP to 2, 5-diamino-6-ribosylamino-4(3H)-pyrimidinone 5'-phosphate (DARP) (Foor and Brown, 1975; Foor and Brown, 1980; Richter et. al., 1993). The DARP further undergoes deamination, side chain reduction, and dephosphorylation to form 4-ribitylamino-5-amino-2,6-dihydroxypyrimidine (RAADP) (Burrows and Brown, 1978; Richter et. al., 1997; Bacher et. al., 1997) catalyzed by pyrimindine deaminase, pyrimidine reductase and a hitherto unknown phosphatase, respectively. Lumazine synthase catalyzes the condensation of RAADP with

DHBP to form 6,7-dimethyl-8-ribityllumazine (DMRL) (Kis and Bacher, 1995; Kis et. al., 1995). The dismutation reaction of two molecules of DMRL results in one molecule of riboflavin and one molecule of RAADP catalyzed by riboflavin synthase (Plaut, 1960; Plaut, 1963; Plaut et. al., 1970; Fischer and Bacher, 2008). Finally, riboflavin is catalyzed to form flavin mononucleotide (FMN) and flavin adenine dinucleotide (FAD) by a bifunctional riboflavin kinase/ FAD synthetase in bacteria (Bacher, 1991).

Solution and crystal structures of DHBPS are available from *Escherichia coli* (Kelly et. al., 2001; Liao et. al., 2001), *Magnaporthe grisea* (Liao et. al., 2002), *Methanococcus jannashii* (Steinbacher et. al., 2003), *Candida albicans* (Echt et. al., 2004) and *Salmonella typhimurium* (Kumar et. al., 2010) where DHBPS is encoded as a single separate polypeptide chain. In all these species, DHBPS exists as a homo-dimer and possess an $\alpha + \beta$ fold with unusual connectivity of β strands. The two monomers interact with each other largely by hydrophobic interactions at the dimer interface through hydrophobic residues. Two topologically equivalent catalytic sites are formed at the dimer interface and the residues involved in catalysis are contributed by both the subunits and conserved throughout the species, reflecting a similar mechanism for the catalysis (Liao et. al., 2001; Liao et. al., 2002; Steinbacher et. al., 2003; Echt et. al., 2004; Kumar et. al., 2010). The studies also revealed that the active site of each monomer is essentially formed by two loops contributed by the residues 34 to 39 (acidic active site loop, *E. coli* numbering) and by the residues 84 to 94 (Tyrosine loop, *E. coli* numbering). The acidic active site loop undergoes a conformational change from open or disordered conformation to a closed ordered conformation upon binding of ribulose-5-phosphate and/or essential divalent metal ions (Steinbacher et. al., 2003; Kumar et. al., 2010). The tyrosine loop, on the other hand plays a role in the active site access to the substrate (Steinbacher et. al., 2003). A proposed catalytic mechanism for DHBPS suggests that the conversion of D-ribulose-5-phosphate to L-DHBP in the presence of divalent metal

ion undergoes a number of catalytic steps such as racemization, enolization, ketonization, dehydration, skeleton rearrangement and formate elimination (Volk and Bacher 1991; Fischer et. al., 2002).

In *Mtb*, both DHBPS and GTPCH-II enzymes are fused together at N- and C-terminal respectively, and encoded by a single *ribA2* gene (Rv1415). The characterization of bi-functional DHBPS/GTPCH-II enzyme has been reported in *Arabidopsis thaliana* and on the basis of DNA sequence similarity, such bi-functional enzymes are also predicted to be present in *Bacillus subtilis*, *Bacillus amyloliquefaciens* and *Synechocystis sp* (Herz et. al., 2000). So far, biochemical and structural characterization of DHBPS are available only from the species where it is encoded as a single polypeptide chain and no reports are yet available where it is encoded as a bi-functional enzyme. Moreover, the complete complex reaction mechanism of DHBPS is not well understood till now. Here, we are reporting the first structural characterization of N-terminal DHBPS domain of pathogenic *Mtb* where it is encoded as a bi-functional enzyme along with GTPCH-II domain. The crystal structures of DHBPS domain of *Mtb* in monomeric and dimeric form may help to understand its molecular mechanism and to exploit its potential as an anti-bacterial drug target.

2. Materials and Methods

2.1. Cloning of Mtb-DHBPS domain

The 618 base pair encoding *Mtb*-DHBPS domain was amplified from the genomic DNA of *M. tuberculosis* (H37Ra) by polymerase chain reaction (PCR) using forward (5'-TAT TAC ACT CAT ATG ACG AGG TTG GAC TCC-3') and reverse (5'-TAT TAC ATT CTC GAG TCA CTC ATG CTT GCG CCG-3') primers (IDT, USA) incorporating *NdeI* and *XhoI* restriction sites respectively. The amplified PCR fragment was purified using gel extraction

kit (Qiagen, Germany) and digested with *NdeI* and *XhoI* enzymes (New England Biolabs, USA) for 15 hours at 37°C. The digested PCR fragment was ligated into pET28c vector (Novagen Inc., USA) which was digested with the same set of restriction enzymes to express the protein with N-terminal 6xhistidine-tag. The insertion of PCR fragment into the vector was confirmed by automated DNA sequencing. The resulting clone (*Mtb*-DHBPS-pET28c) was transformed into *E. coli* BL21 (DE3) strain by calcium chloride treatment for the expression of *Mtb*-DHBPS protein.

2.2. Expression and purification of Mtb-DHBPS domain

A single colony of *Mtb*-DHBPS-pET28c in BL21(DE3) was inoculated in 10 ml of Luria-Bertani (LB) media along with kanamycin (30 μg/ml) and grown overnight at 37°C in an incubator shaker. This overnight seed culture was used to inoculate 1 litre of LB media along with required antibiotic and allowed to grow further at 37°C. The culture was grown till the cell density as monitored by absorbance at 600 nm reached a value of 0.6. At this stage, the *Mtb*-DHBPS protein expression was induced by adding 0.5 mM isopropyl β-D-thiogalactopyranoside (IPTG) and the culture was allowed to grow further at 37°C for 4 hours. The cells were harvested by centrifuging the culture at 5000 rpm for 30 minutes at 4°C. The supernatant was discarded and the cell pellet was resuspended in lysis buffer (50 mM Tris pH 8.0, 150 mM NaCl, 10mM imidazole, 1mM PMSF, 1mg/ml lysozyme) and incubated on ice for 30 minutes followed by the addition of cocktail of protease inhibitors (Sigma, USA). The resuspended cells were lysed using a French press at 1500 psi pressure (SIM-AMINCO, Spectronic Instruments). The cell debris were pelleted by centrifugation at 15000g for 60 minutes at 4°C and the supernatant was loaded onto the Ni-NTA column (Qiagen, Germany), which was pre-equilibrated with lysis buffer (without lysozyme). After passing the supernatant two times through Ni-NTA, the column was washed with 50 mM Tris

pH 8.0, 150 mM NaCl, 40 mM imidazole buffer to remove any unbound proteins. The bound protein was eluted from the column with 50 mM Tris pH 8.0, 150 mM NaCl and 200 mM imidazole buffer. The eluted protein was dialyzed against 20 mM Tris pH 8.0, 150 mM NaCl and 1 mM DTT buffer for overnight at 4°C and further purified by size exclusion chromatography using sephacryl S-200 column (GE Healthcare, USA). The purified protein was further concentrated using Amicon concentrator with 10 kDa molecular weight cutoff membrane (Millipore, USA). The concentration of the protein was estimated by Bradford method (Bradford, 1976) and the purity of the protein was checked by SDS-PAGE (Laemmli, 1970).

2.3. Size-exclusion chromatography

To know the quaternary structure of *Mtb*-DHBPS domain in solution, its hydrodynamic volume was determined using sephacryl S-200 column (GE Healthcare, USA) installed on BIO-RAD Duoflow (BioRad, USA) protein purification system. The *Mtb*-DHBPS and standard molecular weight markers (Sigma, USA) were prepared separately in the buffers containing potassium phosphate buffer pH 6.0, 150 mM NaCl, 1 mM DTT and 50 mM sodium acetate pH 4.0, 150 mM NaCl, 1 mM DTT. The concentrated *Mtb*-DHBPS protein was passed through S-200 column and the elution profile was compared with the standard molecular weight marker profile to estimate the size of protein in solution.

2.4. Circular dichroism analysis

Circular dichroism (CD) data measurements were made on a Jasco J-810 spectropolarimeter using 0.2 mg/ml concentration of purified *Mtb*-DHBPS in cuvettes of path length 0.1 cm, and scanning raw ellipticity (θ) values in the range of 250 to 198 nm with nitrogen gas flowing at 6-9 liters per minute at 25°C. For pH based scans, *Mtb*-DHBPS was

concentrated to 10 mg/ml and diluted in different buffers of 50 mM strength with different pH values to a concentration of 0.2 mg/ml. The pH values are obtained by using the buffer, sodium citrate/citric acid for pH 3.0, sodium acetate/acetic acid for pH 4.0 and pH 5.0, potassium phosphate buffer for pH 6.0 and pH 7.0, Tris buffer for pH 8.0, CHES buffer for pH 9.0 and CAPS buffer for pH 10.0. For the pH-dependent temperature scans, raw observed ellipticity values were measured at a fixed wavelength of 222 nm. For standard wavelength scans, raw θ values were converted to mean residue ellipticity values using the formula, [θ] = {θobs x 100 x mean residue weight} / {concentration (mg/ml) x path length (cm)}.

2.5. Measurement of Mtb-DHBPS enzyme activity

The *Mtb*-DHBPS enzyme activity was measured by a colorimetric method using Picollelli et al., protocol (Picollelli et. al., 2000). Briefly, in 125 µl reaction volume, 15 µg of *Mtb*-DHBPS was mixed with 50 mM Tris-HCl buffer (pH 7.5), 5 mM $MgCl_2$, 5 mM D-ribose-5-phosphate and 0.25 units of pentose phosphate isomerase (PPI) (Sigma, USA) and incubated at 37°C for 30 minutes. The enzyme reaction was quenched and colour was formed by addition of 100 µl of saturated creatine solution followed by 50 µl of α-naphthol (35 mg/ml in 1.0 N NaOH). The colour was allowed to develop for 30 minutes before measuring the absorbance at 525 nm using ELISA plate reader (BIOTEK power wave XS plate reader). The values were compared to the standard plot that was established with 0-50 nmol of 2, 3-butadione per 125 µl reaction volume and treating them as above for the colour development. To measure the activity of *Mtb*-DHBPS at different pH values, the reaction was carried out individually with 50 mM sodium citrate (pH 3.0), 50 mM sodium acetate (pH 4.0 and pH 5.0), 50 mM potassium phosphate (pH 6.0 and pH 7.0), 50 mM Tris-HCl (pH 8.0), 50 mM CHES (pH 9.0), 50 mM CAPS (pH 10.0) buffers. The reversibility of the enzyme activity was measured by dialyzing the protein at pH 5.0 overnight and checked the quaternary

structure by size-exclusion chromatography studies. The enzyme was dialyzed again at pH 8.0 overnight and measured the enzyme activity at optimal pH.

2.6. Crystallization

The purified *Mtb*-DHBPS (12 mg/ml) in 20 mM Tris pH 8.0, 150 mM NaCl and 1 mM DTT was used for crystallization by sitting drop vapour diffusion method in 96 wells plate (MRC Plates, Molecular Dimensions, UK). Initial crystallization screens was carried out using commercially available screen kits from Qiagen (Classic Suite) and Hampton Research (PEG-Ion Screen) by mixing 1 µl of protein solution with 1 µl of reservoir buffer equilibrating against 60 µl of precipitant solution and incubated at 20°C. The final diffractable quality crystal at pH 6.0 was obtained within two days by using 0.1 M potassium phosphate (pH 6.0) and 20% PEG3350 as reservoir solution. Similarly, the crystal at pH 4.0 was obtained by mixing 0.5 M ammonium sulphate, 15% PEG4000, 0.1 M sodium acetate buffer (pH 4.0) with equal amount of protein and incubated at 20°C. The crystals grew after 15-20 days in sitting drop condition. The *Mtb*-DHBPS-Zn-SO_4 complex crystal was obtained by soaking the crystal grown at pH 4.0 overnight in 20 mM zinc chloride.

2.7. Data collection and processing

X-ray diffraction data set for the crystal obtained at pH 6.0 was collected at 100 K using synchrotron radiation (BM14 beam line, ESRF, France). Prior to diffraction, crystals were cryo-protected by soaking them in a solution of 20% glycerol added to their mother liquor. For the crystals obtained at pH 4.0 and soaked with zinc chloride, the X-ray diffraction data sets at 100 K were collected in an in-house MAR345 image plate detector mounted on Rigaku MicroMax-007HF rotating anode generator operated at 40 kV and 30 mA. All the diffraction images were indexed, integrated and scaled using *HKL2000* suite of programs

(Otwinowski and Minor, 1997). The scaled intensities were converted into structure factors using the program *TRUNCATE* (French and Wilson, 1978) as implemented in *CCP4* (CCP4, 1994).

2.8. Structure determination and refinement

For the crystal obtained at pH 6.0, the structure was solved by molecular replacement method using *PHASER* (McCoy et. al., 2007) program with DHBPS monomer from *E. coli* (Liao et. Al., 2001) as search model (PDB ID: 1G57). The final solution of *PHASER* yielded two molecules per asymmetric unit with Log (Likelihood) Gain score of 1615.51. The initial model was refined as rigid body followed by restraint refinement using *REFMAC5* (Murshudov et. al., 1997) program. The *Mtb*-DHBPS model was built into the electron density map using the program *COOT* (Emsley and Cowtan, 2004). Solvent molecules were added manually in the difference Fourier (F_o-F_c) electron density map if they had values more than 3σ above the mean and formed at least one hydrogen bond with either protein or solvent atom. Similarly, for the crystal obtained at pH 4.0, the structure was solved by molecular replacement using *PHASER* program with *Mtb*-DHBPS monomer as search model. The initial model was refined and built using *REFMAC5* and *COOT* programs respectively. For the zinc-sulphate complex, the structure was solved by rigid body refinement using *Mtb*-DHBPS as the starting model and refined using *REFMAC5*. All the models were validated using *PROCHECK* (Laskowski et. al., 1993) program as implemented in *CCP4*. All the coordinates and structure factors are submitted to Protein Data Bank (PDB) with PDBID's 3MIO (pH 6.0), 3MGZ (pH 4.0) and 3MK5 (pH 4.0+Zn).

3. Results and discussion

3.1. Cloning, expression and purification of Mtb-DHBPS domain

The length of the N-terminal *Mtb*-DHBPS and C-terminal GTPCH-II domains were determined by aligning the ribA2 amino acid sequence of *Mtb* with DHBPS sequences from various species (Fig. 2) and by the pairwise alignment of amino acid sequences between ribA2 of *Mtb* and GTPCH-II of *E. coli* (Ren et. al., 2005) for which the crystal structure is available. Based on the sequence alignment, the amino acid residues from 1-206 and the residues from 207-425 of ribA2 were considered as N-terminal DHBPS domain and C-terminal GTPCH-II domain, respectively. The 618 base pairs encoding the N-terminal DHBPS domain of *Mtb* was amplified by PCR, cloned into pET28c vector and expressed in *E. coli* with 6xhistidine-tag at the N-terminal of *Mtb*-DHBPS domain. The expressed protein was purified by affinity chromatography followed by size exclusion chromatography.

3.2. Characterization of Mtb-DHBPS domain

As this is the first time, a DHBPS enzyme has been recombinantly expressed and purified from a bi-functional enzyme, we have investigated the biophysical and biochemical characterization of *Mtb*-DHBPS domain to compare it with other DHBPS enzymes which are encoded as a separate polypeptide chain. The size exclusion chromatography studies showed that at pH 8.0, the *Mtb*-DHBPS domain elutes as a dimer (Fig. 3A) suggesting that the enzyme is dimer in solution as observed in other species. The CD spectra of *Mtb*-DHBPS domain at pH 8.0 showed that the enzyme is well folded consisting of α-helix and β-sheets (Fig. 3B) and exhibited activity in the presence of magnesium ion as reported in other species (Liao et. al., 2001; Liao et. al., 2002; Steinbacher et. al., 2003; Echt et. al., 2004; Kumar et. al., 2010). To determine the optimal pH as part of biochemical characterization, the activity

of *Mtb*-DHBPS was measured at different pH values. The *Mtb*-DHBPS showed maximum activity at pH 7.5, but, lost its activity when the pH is below 5.0 and above 9.0 (Fig. 3C). Surprisingly, the CD spectra observed at pH values from 3.0 – 10.0 (Fig. 3D) does not show any significant change suggesting the secondary structure content remains same even at the acidic and basic pH values. However, the size-exclusion chromatography studies showed that the *Mtb*-DHBPS forms a dimer in solution between the pH 6.0 – 9.0, and the majority of the protein was found to be in monomer form at pH 4.0 (Fig. 3E). Moreover, the melting studies of *Mtb*-DHBPS suggests that it unfolds at about 65°C between the pH 6.0 – 8.0, while at pH 4.0, it does not show any significant unfolding even at a temperature of 95°C indicating a higher structural stability than it is at pH 6.0 – 8.0 (Fig. 3F). Further, the functional activity of *Mtb*-DHBPS domain could be restored up to 70% by changing the pH of the enzyme by dialysis from pH 5.0 to pH 8.0. The dialyzed enzyme also showed dimeric form in size-exclusion chromatography studies at pH 8.0. Thus, these results suggest that the loss of *Mtb*-DHBPS activity at pH 4.0 is due its inability to form dimer in solution as it has been shown that the biologically active form of DHBPS is dimer both in solution as well as in crystal structures.

3.3. Crystal structure of Mtb-DHBPS domain at pH 6.0

To understand the structural details we have crystallized *Mtb*-DHBPS domain at pH 6.0 in monoclinic C2 space group and the X-ray diffraction data were collected up to 1.8 Å resolution. Assuming the molecular weight of *Mtb*-DHBPS is 22400 Da (as determined by MALDI studies) and two molecules per asymmetric unit, the calculated V_M (Matthews coefficient) value (Matthews, 1968) and solvent content corresponds to 2.26 $Å^3$ Da^{-1} and 45.66 %, respectively, which are expected values for a protein crystal. The *Mtb*-DHBPS structure was solved by molecular replacement method using *E. coli* DHBPS (PDB ID:

1G57) as search model and refined to an R-factor of 18.7% and free-R of 23.3%. The residues from 75 – 85 in A chain and residues from 75 – 86 in B chain monomers could not be traced in the electron density map and are not included in the model. The final model thus consists of 389 residues, 3 phosphate ions, 6 glycerol molecules, 2 potassium ions and 369 solvent molecules. The Ramachandran plot analysis using *PROCHECK* (Laskowski et. al., 1993) program for the refined model shows 94.9% of the amino acid residues are in most favoured region, and 5.1% are in the additionally allowed region. The final refinement statistics are shown in Table 1.

The overall three-dimensional structure of *Mtb*-DHBPS domain represents an α+β fold as reported in other species (Liao et. al., 2001; Liao et. al., 2002; Steinbacher et. al., 2003; Echt et. al., 2004; Kumar et. al., 2010) with seven helices surrounding the central eight-stranded β-sheet core (Fig. 4A). All the β-strands are either parallel or anti-parallel to each other and interconnected by a cross-over consisting of loop or helix. Although, the asymmetric unit consists of two molecules of *Mtb*-DHBPS, the functional homo-dimer would be generated by applying a crystallographic two-fold rotational symmetry to the A chain monomer (Fig. 4B). The buried surface area calculated using PISA server (Krissinel and Henrick, 2007) for the functional homo-dimer is 2150 $Å^2$ (11.9% per monomer), suggesting a stable homo-dimer complex between the molecules across the asymmetric unit. The two subunits forming homo dimer interacts with each other largely through hydrogen bond interactions, which is in contrast with the earlier reported structures where the two subunits interact with each other largely through hydrophobic interactions (Liao et. al., 2001; Liao et. al., 2002; Steinbacher et. al., 2003; Echt et. al., 2004; Kumar et. al., 2010). Analysis of the amino acid sequences revealed that the residues responsible for the hydrophobic interactions are mutated mostly to Tyrosine residue in *Mtb*-DHBPS (Fig. 2). For example, the Ile-65, Val-84 and Phe-95 (*E.*

coli numbering) residues in *E. coli* which are contributing to the hydrophobic interactions are all mutated to Tyrosine residues (Tyr-56, Tyr-75 and Tyr-86) in *Mtb*-DHBPS.

The two subunits of the functional homo-dimer interact with each other through several hydrogen bond interactions. The residues Glu-31, Ser-54, Thr-87, Thr-89, Ser-103, Arg-105 and Gly-173 from one subunit forms hydrogen bonds with the residues Thr-98, Arg-105, Thr-89, Thr-87, Glu-31, Gly-173, Ser-54 and Ser-103 of other subunit, respectively. In addition, the dimer formed in the asymmetric unit also interacts with each other mostly through electrostatic interactions. The residues Asp-62, Asp-135, Arg-153, Arg-202 of one subunit interacts with Arg-153, Arg-202, Asp-62, Asp-135 of other subunit, respectively.

The catalytic site at the dimeric interface was bound with a glycerol and phosphate molecules (Fig. 4C). Both the glycerol and phosphate molecules mimic the substrate ribulose-5-phosphate and a similar structure was reported for *M. grisea* (Liao et. al., 2002). The phosphate molecule is stabilized in its position by hydrogen bonding through its O1 atom with O1 of glycerol and with OD2 of Asp33 through a water molecule; O2 atom with NH2 of Arg141; O3 atom with N of His144 and to a water molecule; O4 atom with NH1 of Arg141 and OG1 of Thr145. The phosphate molecule occupies the same position at the active site as the phosphate moiety of ribulose-5-phosphate and this position is found to be conserved throughout the species (Liao et. al., 2002; Steinbacher et. al., 2003; Echt et. al., 2004; Kumar et. al., 2010). Similarly, the glycerol molecule is stabilized in its position by forming hydrogen bond between O1 and O1 of phosphate ion, O2 and O3 with NE2 of His127 of the opposite monomer. However, the orientation of the glycerol molecule is different in *Mtb*-DHBPS than the one observed in *M. grisea* possibly because of the absence of any divalent metal ions at the active site.

Superposition of *Mtb*-DHBPS with other structurally known DHBPS structures revealed that the overall fold is similar suggesting that the reaction mechanism will also remain the

same. However, the orientation of first loop (loop1) from residues 24-31 is observed in open conformation similar to the one observed in *C. albicans* (Echt et. al., 2004), the second loop (loop2) from residues 74-86 is disordered in *Mtb*-DHBPS and the third loop (loop3) from residues 165-177 is observed in different orientation (Fig. 4D). The loop1 (acidic active site loop) has been shown to play a role in binding the substrate ribulose-5-phosphate and divalent metal ions and undergoes a conformational change from open conformation to the closed conformation upon binding of substrate and/or metal ions (Liao et. al., 2002; Steinbacher et. al., 2003) at the active site. The loop2, which is disordered in *Mtb*-DHBPS, has been suggested to a play role in substrate delivery at the active site (Steinbacher et. al. 2003). The loop3 which is an ordered flexible loop does not have any known function till now.

3.4. Crystal structures of Mtb-DHBPS domain at pH 4.0

To understand the molecular mechanism of higher structural stability shown by *Mtb*-DHBPS at low pH, we have crystallized the *Mtb*-DHBPS domain at pH 4.0 in hexagonal $P6_1$ space group and the X-ray diffraction data were collected up to 2.08 Å resolution. Assuming the molecular weight of *Mtb*-DHBPS is 24200 Da and one molecule per asymmetric unit, the calculated V_M (Matthews coefficient) value and solvent content corresponds to 2.30 $Å^3$ Da^{-1} and 46.49 %, respectively, which are within the range of expected values for protein crystals. The structure was solved by molecular replacement method using a monomer of dimeric *Mtb*-DHBPS structure as a search model and refined to a R-factor of 19% and free-R of 23.8%. The residues from 26 – 27, 74 – 85 and 169 – 174 could not be traced in the electron density map and thus not included in the model. Of the two, one sulphate molecule was found at the active site and occupied a similar position as phosphate in dimeric form of *Mtb*-DHBPS. The final model thus consists of 186 amino acid residues, two sulphate ions and

111 solvent molecules. The Ramachandran plot analysis using *PROCHECK* program for the refined model shows 97.4% of the amino acid residues are in most favoured region and 2.6% are in additionally allowed region. The final refinement statistics are shown in Table 1.

To know whether the monomeric *Mtb*-DHBPS can still bind divalent metal ions, we soaked the crystals grown at pH 4.0 with 20 mM zinc chloride overnight and collected the X-ray diffraction data up to 2.08 Å resolution. The crystal soaked with zinc also belonged to $P6_1$ space group with one molecule per asymmetric unit and the structure was solved using the structure of *Mtb*-DHBPS monomer. The residues from 28 – 30, 75 – 85 and 169 – 170 are not included in the model due to poor electron density. The difference Fourier electron density (F_o-F_c) map clearly showed an extra electron density at 5.0σ level at two sites, which were modeled as zinc ions. The data collection and refinement statistics are shown in Table 1.

The overall three-dimensional structure of *Mtb*-DHBPS at pH 4.0 is similar to the one observed at pH 6.0 (Fig. 5A). The analysis of crystal packing and the prediction of assembly formation using PISA server revealed that the *Mtb*-DHBPS at pH 4.0 forms only a monomer. The monomeric form of *Mtb*-DHBPS at pH 4.0 in solution was also confirmed by the size exclusion chromatography studies. In the Mtb-DHBPS-Zn complex structure, the first zinc ion was located at the active site coordinating with His-144 and the sulphate ion while the second zinc ion was located at the outer surface of the molecule coordinating with His-188 (Fig. 5B). However, the high temperature factor for Zn ions suggests that they have less occupancy at their respective sites. Nevertheless, the first zinc ion located at the active site occupied the conserved divalent metal ion position as reported in other species (Liao et. al., 2002; Steinbacher et. al., 2003; Echt et. al., 2004; Kumar et. al., 2010). The superposition of monomeric *Mtb*-DHBPS structure with and without zinc ion revealed that the overall

structure is similar with root mean square (r.m.s.) deviation of 0.23 Å for 183 C^{α} atoms (Fig. 5C).

3.5. Mechanism of pH dependent monomer-dimer transition of Mtb-DHBPS domain

To understand the molecular mechanism of pH dependent monomer-dimer transition, we have superimposed the *Mtb*-DHBPS structures determined at pH 6.0 and pH 4.0. The superposition revealed that the overall three-dimensional structures in both forms are similar with r.m.s. deviation of 0.70 Å for 176 C^{α} atoms as calculated by LSQMAN program (Kleywegt and Jones; 1995) (Fig. 6A). However, a significant difference was observed in the conformation of loop3 formed by the residues 165-177. The residues from 165-177 forms a loop in the dimeric *Mtb*-DHBPS structure, while, it is observed as a helix for the residues 174-177, thereby increasing the length of the α6-helix from 15 to 22 Å and rest of it is observed as a disordered loop (165-174) in monomeric *Mtb*-DHBPS structure (Fig. 6B). The superposition of *Mtb*-DHPBS monomer structure on the DHBPS structures from *C. albicans*, *M. jannaschii* and *M. grisea* revealed that the length of the α6-helix in monomeric *Mtb*-DHBPS is higher than rest of the structures (Fig. 6C). The transition of loop to helix conformation for the residues from 174-177 results in a loss of hydrogen bond interaction between the carbonyl oxygen of Gly-173 of one subunit with amide atom of Ala-102 from another subunit in dimeric form. Notably, these residues- Gly-173 and Ala-102 are conserved among all the species for which the structures are available till now except in *M. janaschii*. Moreover, increase in the length of α6-helix causes a steric clash with the acidic loop (loop1) causing it to move into a closed conformation (Fig. 6B). It was observed earlier that the acidic loop was found in open or disordered conformation in the absence of any substrate or metal ions and tends to close only upon substrate and/or metal ion binding (Steinbacher et.

al., 2003). However, in *Mtb*-DHBPS structure at pH 4.0, the acidic loop is found in almost closed conformation in the absence of any substrate binding.

Based on our results, we propose a model for the loss of dimerization of *Mtb*-DHBPS domain at low pH. *Mtb*-DHBPS domain is observed in a dimeric form between the pH 6.0-9.0 by forming hydrogen bond and ionic interactions between the subunits. At pH 5.0 and below, these ionic and hydrogen bond interactions between the subunits are lost depending upon the ionization state of the residues at the dimeric interface resulting in the formation of monomer and thus, loss of activity. Expectedly, the loss of a conserved hydrogen bond formed by Gly-173 and Ala-102 between the two subunits causes more flexibility in the conformation of loop3 formed by the residues 165-177. This conformational flexibility of loop3 allows the residues 174-177 (SMAH) to transit from loop to helix as observed in monomeric structure obtained at pH 4.0. However, as the pH is increased to 6.0 and above, the residues 174-177 (SMAH) tend to form an ordered loop, making the backbone of residues available for a hydrogen bond interaction between two subunits, leading to formation of a dimer and thus, showing enzyme activity of *Mtb*-DHBPS. The helix-loop transition is supported by the fact that average temperature factor for the residues 174-177 (SMAH) at pH 4.0 is about 68.3 Å (average temperature factor of the protein is 41.3 Å) while the average temperature factor for the same residues at pH 6.0 is about 18.8 Å (average temperature factor for the protein is 21.7 Å), indicating a flexibility in the conformation of helix formed by the residues 174-177 at pH 4.0. Since the amino acid residues of 'SMAH' are observed only in *Mtb*-DHBPS domain, we speculate that this observation is unique for *Mtb*-DHBPS domain.

4. Conclusions

M. tuberculosis is a successful pathogen in humans and may need to survive in stress including the change in environmental pH. The present work describes the first characterization of DHBPS domain of a bi-functional DHBPS/GTPCH-II enzyme from *Mtb*. The *Mtb*-DHBPS domain shows activity independently and is optimally active at pH 7.5. The characterization of this domain revealed that the enzyme shows activity between pH 6.0 to 9.0 and forms a dimer in solution as well in the crystal structure. However, at pH 5.0 and below, it forms inactive stable monomer in solution as well as in crystal structure. Moreover, the activity and dimerization could be reversed by increasing the pH to 6.0-9.0 of *Mtb*-DHBPS. These results suggest that the *Mtb*-DHBPS domain can transit between monomer and dimer depending upon its pH values. The crystal structure determined at pH 6.0 shows that *Mtb*-DHBPS forms a dimer and the residues from 165 to 177 exhibits a loop conformation. However, the crystal structure determined at pH 4.0 shows that *Mtb*-DHBPS forms a monomer and the residues from 174 to 177 forms a turn and becomes part of α6-helix. The increase in α6-helix length causes the acidic loop to be observed in closed conformation which is otherwise will have steric clash with α6-helix. Thus, *Mtb*-DHBPS domain shows reversible dimer-monomer transition or active to inactive form depending on its pH value, in *in vitro*. However, the present structure represents only the DHBPS domain of *Mtb* and further work is required to validate the results obtained here for the full length protein with both GTPCH-II and DHBPS domains for its biological significance. Nevertheless, this is a first report for a DHBPS enzyme where it is shown to transit between monomer-dimer forms by structural changes depending on its pH values. As DHBPS enzyme is essential for the survival of the *Mtb* and considered it as a potential drug target the results presented here may help in designing the species specific antibacterial drug against this target.

Acknowledgements

We thank Dr. Hassan Belhrali for his help during data collection at ESRF, France and Dr. Purnananda Guptasarma for his help in carrying out the MALDI and CD analysis. M. S. and P. K. thanks the Council of Scientific and Industrial Research (CSIR), Government of India, for doctoral fellowships. We thank Dr. Srikrishna Subramanian and Dr. Balvinder Singh for carefully reading the manuscript. This work was supported by CSIR through network project SIP10. We also thank Department of Biotechnology, Government of India for the financial assistance provided for the data collection in France.

REFERENCES

Bacher, A., 1991. Riboflavin kinase and FAD synthetase. In: Muller F, editor. Chemistry and biochemistry of flavoenzymes. London: CRC press pp 349–370.

Bacher, A., Richter, G., Ritz, H., Eberhardt, S., Fischer, M., Krieger, C., 1997. Biosynthesis of riboflavin: GTP cyclohydro-lase II, deaminase and reductase. Methods in Enzymology 280, 382-389.

Bradford, M.M., 1976. A rapid and sensitive method for the quantitation of microgram quantitites of protein utilizing the principle of protein-dye binding. Anal. Biochem. 72, 248–254.

Burrows, R.B., Brown, G.M., 1978. Presence of Escherichia coli of a deaminase and a reductase involved in biosynthesis of riboflavin. J. Bacteriol. 136, 657-667.

Cole, S.T., Eiglmeier, K., Parkhill, J., James, K.D., Thomson, N.R., Wheeler, P.R., Honoré, N., Garnier, T., Churcher, C., Harris, D., Mungall, K., Basham, D., Brown, D., Chillingworth, T., Connor, R., Davies, R.M., Devlin, K., Duthoy, S., Feltwell, T., Fraser, A., Hamlin, N., Holroyd, S., Hornsby, T., Jagels, K., Lacroix, C., Maclean, J., Moule, S., Murphy, L., Oliver, K., Quail, M.A., Rajandream, M.A., Rutherford, K.M., Rutter, S., Seeger, K., Simon, S., Simmonds, M., Skelton, J., Squares, R., Squares, S., Stevens, K., Taylor, K., Whitehead, S., Woodward, J.R., Barrell, B.G., 2001. Massive gene decay in the leprosy bacillus. Nature 409, 1007-1011.

Collaborative Computational Project Number 4, 1994. The CCP4 suite: programs for protein crystallography. Acta Crystallogr. D 50-760–763.

Echt, S., Bauer, S., Steinbacher, S., Huber, R., Bacher, A., Fischer, M., 2004. Potential anti-infective targets in pathogenic yeasts: structure and properties of 3,4-dihydroxy-2-butanone 4-phosphate synthase of Candida albicans. J. Mol. Biol. 341, 1085-1096.

Emsley, P., Cowtan, K., 2004. Coot: model-building tools for molecular graphics. Acta Crystallogr. D 60, 2126–2132.

Fischer, M., Bacher, A., 2008. Biosynthesis of vitamin B2: Structure and mechanism of riboflavin synthase. Arch. Biochem. Biophys. 474, 252-265.

Fischer, M., Romisch, W., Schiffmann, S., Kelly, M., Oschkinat, H., Steinbacher, S., Huber, R., Eisenreich, W., Richter, G., Bacher, A., 2002. Biosynthesis of riboflavin in archaea: studies on the mechanism of 3, 4-dihydroxy-2-butanone-4-phosphate synthase of Methanococcus jannaschii. J. Biol. Chem. 277, 41410-41416.

Foor, F., Brown, G.M., 1975. Purification and properties of guanosine triphosphate cyclohydrolase II from Escherichia coli. J. Biol. Chem. 250, 3545-3551.

Foor, F., Brown, G.M., 1980. GTP cyclohydrolase II from Escherichia coli. Methods in Enzymology 66, 303-307.

French, G.S., Wilson, K.S., 1978. On the treatment of negative intensity observations. Acta. Cryst. A34, 517-525.

Gerdes, S.Y., Scholle, M.D., D'Souza, M., Bernal, A., Baev, M.V., Farrell, M., Kurnasov, O.V., Daugherty, M.D., Mseeh, F., Polanuyer, B.M., Campbell, J.W., Anantha, S., Shatalin, K.Y., Chowdhury, S.A., Fonstein, M.Y., Osterman, A.L., 2002. From genetic footprinting to antimicrobial drug targets: examples in cofactor biosynthetic pathways. J. Bacteriol. 184, 4555-4572.

Herz, S., Eberhardt, S., Bacher, A., 2000. Biosynthesis of riboflavin in plants. The ribA gene of Arabidopsis thaliana specifies a bifunctional GTP cyclohydrolase II/3,4-dihydroxy-2-butanone 4-phosphate synthase. Phytochemistry 53, 723-731.

Kelly, M.J., Ball, L.J., Krieger, C., Yu, Y., Fischer, M., Schiffmann, S., Schmieder, P., Kühne, R., Bermel, W., Bacher, A., Richter, G., Oschkinat, H., 2001. The NMR structure of the 47-kDa dimeric enzyme 3,4-dihydroxy-2-butanone-4-phosphate synthase and ligand binding studies reveal the location of the active site. Proc. Natl. Acad. Sci. U S A. 98, 13025-30.

Kis, K., Bacher, A., 1995. Substrate channeling in the lumazine synthase/riboflavin synthase complex of Bacillus subtilis. J. Biol. Chem. 270, 16788-16795.

Kis, K., Volk, R., Bacher, A., 1995. Biosynthesis of riboflavin. Studies on the reaction mechanism of 6, 7-dimethyl-8-ribityllumazine synthase. Biochemistry 34, 2883-2892.

Kleywegt, G.J., Jones,T.A., 1995. Where freedom is given, liberties are taken. Structure, 3, 535–540.

Krissinel, E., Henrick, K., 2007. Inference of macromolecular assemblies from crystalline state. J. Mol. Biol. 372, 774–797

Kumar, P., Singh, M., Gautam, R., Karthikeyan, S., July 30, 2010. Potential anti-bacterial drug target: Structural characterization of 3,4-dihydroxy-2-butanone-4-phosphate synthase from Salmonella typhimurium LT2. Proteins: Struct., Funct., Bioinf. / 20806221 [Epub ahead of print].

Laemmli, U. K., 1970. Cleavage of structural proteins during the assembly of the head of bacteriophage T4. Nature 227, 680-685.

Laskowski, R.A., MacArthur, M.W., Moss, D.S., Thornton, J.M., 1993. Procheck-a program to check the stereochemical quality of protein structures. J. App. Crystallogr. 26 283-291.

Liao, D.I., Calabrese, J.C., Wawrzak, Z., Viitanen, P.V., Jordan, D.B., 2001. Crystal structure of 3, 4-dihydroxy-2-butanone 4-phosphate synthase of riboflavin biosynthesis. Structure 9, 11-18.

Liao, D.I., Zheng, Y.J., Viitanen, P.V., Jordan, D.B., 2002. Structural definition of the active site and catalytic mechanism of 3, 4-dihydroxy-2-butanone-4-phosphate synthase. Biochemistry 41, 1795-1806.

Matthews, B.W., 1968. Solvent content of protein crystals. J. Mol. Biol. 33, 491-497.

McCoy, A.J., Grosse-Kunstleve, R.W., Adams, P.D., Winn, M.D., Storoni, L.C., Read, R.J., 2007. Phaser crystallographic software. J. Appl. Crystallogr. 40 658–674.

Murshudov, G.N., Vagin, A.A., Dodson, E.J., 1997. Refinement of macromolecular structures by the maximum-likelihood method. Acta Crystallogr. D 53, 240–255.

Oltmanns, O., Bacher, A., 1972. Biosynthesis of ribofavin in *Saccharomyces cerevisiae*: the role of genes rib1 and rib7. J. Bacteriol. 110, 818-822.

Otwinowski, Z., Minor, W., 1997. Processing of X-ray diffraction data collected in oscillation mode. In: Carter, C.W., Sweet, R.M. (Eds.), Methods in Enzymology 276, Macromolecular Crystallography, partA. Academic Press, New York, pp. 307–326.

Philipp, W. J., Poulet, S., Eiglmeier, K., Pascopella, L., Balasubramanian, V., Heym, B., Bergh, S., Bloom, B. R., Jacobs, W. R. Jr., Cole, S. T., 1996. An integrated map of the genome of the tubercle bacillus Mycobacterium tuberculosis H37Rv, and comparison with Mycobacterium leprae. Proc. Natl. Acad. Sci. USA 93, 3132-3137.

Picollelli, M.A., Viitanen, P.V., Jordan, D.B., 2000. Spectrophotometric determination of 3, 4-dihydroxy-2-butanone-4-phosphate synthase activity. Anal. Biochem. 287, 347–349.

Plaut, G.W.E., 1960. Studies on the stoichiometry of the enzymic conversion of 6, 7-dimethyl-8-ribityllumazine to riboflavin.J. Biol. Chem. 235, 41-42.

Plaut, G.W.E., 1963. Studies on the nature of the enzymic conversion of 6,7-dimethyl-8-ribityllumazine to riboflavin. J. Biol. Chem. 238, 2225-2243.

Plaut, G.W.E., Beach, R.L., Aogaichi, T., 1970. Studies on the mechanism of elimination of protons from the methyl groups of 6, 7-dimethyl-8-ribityllumazine by riboflavin synthetase. Biochemistry 9, 771-785.

Ren, J., Kotaka, M., Lockyer, M., Lamb, H.K., Hawkins, A.R., Stammers, D.K., 2005. GTP cyclohydrolase II structure and mechanism. J. Biol. Chem. 280, 36912-36919.

Richter, G., Fischer, M., Krieger, C., Eberhardt, S., Lüttgen, H., Gerstenschläger, I., Bacher, A., 1997. Biosynthesis of riboflavin: characterization of the bifunctional deaminase-reductase of Escherichia coli and Bacillus subtilis. J. Bacteriol. 179, 2022-2028.

Richter, G., Ritz, H., Katzenmeier, G., Volk, R., Kohnle, A., Lottspeich, F., Allendorf, D., Bacher, A., 1993. Biosynthesis of riboflavin: cloning, sequencing, mapping, and expression of the gene coding for GTP cyclohydrolase II in Escherichia coli. J. Bacteriol. 175, 4045-4051.

Richter, G., Volk, R., Krieger, C., Lahm, H.-W., Roethlisberger, U., Bacher, A., 1992. Biosynthesis of ribofavin. Cloning, sequencing and expression of the gene coding for 3,4-dihydroxy-2-butanone 4-phosphate synthase of *Escherichia coli*. J. Bacteriol. 174 4050-4056.

Russell, D.G., Barry, C.E.3rd., Flynn, J.L., 2010. Tuberculosis: what we don't know can, and does, hurt us. Science 328, 852-856.

Sassetti, C.M., Boyd, D.H., Rubin, E.J., 2003. Genes required for mycobacterial growth defined by high density mutagenesis. Mol. Microbiol. 48, 77-84.

Steinbacher, S., Schiffmann, S., Richter, G., Huber, R., Bacher, A., Fischer, M., 2003. Structure of 3,4-dihydroxy-2-butanone 4-phosphate synthase from Methanococcus jannaschii in complex with divalent metal ions and the substrate ribulose 5-phosphate: implications for the catalytic mechanism. J. Biol. Chem. 278, 42256-42265

Vandal, O. H., Nathan, C. F., Ehrt, S., 2009. Acid resistance in Mycobacterium tuberculosis. J. Bacteriol. 191, 4714-4721.

Volk, R., Bacher, A., 1990. Studies on the 4-carbon precursor in the biosynthesis of riboflavin. Purification and properties of L-3, 4-dihydroxy-2-butanone-4-phosphate synthase. J. Biol. Chem. 265, 19479-19485.

Volk, R., Bacher, A., 1991. Biosynthesis of riboflavin. Studies on the mechanism of L-3, 4-dihydroxy-2-butanone 4-phosphate synthase. J. Biol. Chem. 266, 20610-20618.

World health organization (WHO) WHO report 2010: Global tuberculosis control: retrieved on 13th april 2009.

Figure Legends

Fig. 1. Reaction mechanism catalyzed by DHBPS enzyme. *Mtb*-DHBPS catalyze the formation of 3,4-dihydroxy-2-butanone 4-phosphate and formate (products) in the presence of magnesium ion from ribulose-5-phosphate (substrate).

Fig. 2. Multiple sequence alignment of DHBPS/GTPCH-II. (A) Multiple sequence alignment of *Mtb*-DHBPS domain with other species. Residues involved in catalysis are shown in grey, residues involved in hydrogen bond and hydrophobic interactions for the functional dimer are shown in yellow and cyan respectively, residues which are involved in both hydrogen bond interaction and catalysis are shown in magenta and residues involved in electrostatic interactions in asymmetric unit dimer are shown in blue. Residues involved in Loop1, Loop2 and Loop3 formation are marked. Residues involved in the transition of loop to helix (α6) are shown in dotted lines. (B) Multiple sequence alignment of *Mtb*-GTPCH-II domain with other species. Conserved residues are shown in yellow.

Fig. 3. Characterization of *Mtb*-DHBPS domain. (A) Size-exclusion chromatography elution profile of *Mtb*-DHBPS domain at pH 8.0. (B) Far-UV circular dichroism spectra for *Mtb*-DHBPS domain at pH 8.0. (C) Enzyme activity of *Mtb*-DHBPS domain from pH 4.0 – 10.0. (D) Far-UV circular dichroism spectra of *Mtb*-DHBPS domain from pH 3.0 – 9.0. (E) Size-exclusion chromatography elution profile of *Mtb*-DHBPS domain at pH 6.0 (black) and pH 4.0 (red). (F) Melting CD spectra of Mtb-DHBPS domain at pH 8.0 (green), pH 6.0 (red) and pH 4.0 (black).

Fig. 4. Crystal structure of *Mtb*-DHBPS domain at pH 6.0. (A) Cartoon diagram showing the *Mtb*-DHBPS monomer with secondary structure elements labeled. The α-helices are shown in red, β-strands are in yellow and loops are in green. (B) Cartoon diagram representing the functional homo-dimer (green and red) of *Mtb*-DHBPS domain created by applying crystallographic two-fold rotational symmetry at pH 6.0. The glycerol and phosphate molecules bound at the dimer interface are shown in stick model. (C) Stereoview showing the final $2F_o$-F_c electron density map covering glycerol and phosphate molecule is contoured at 1.0 σ level. Residues

marked in red are from the neighbouring subunit. The interactions are shown in dotted lines. (D) Superposition of DHBPS monomers from *M. tuberculosis* (green), *C. albicans* (pink), *M. jannaschii* (yellow) and *M. grisea* (magenta) showing three loops in different orientations.

Fig. 5. Crystal structure of *Mtb*-DHBPS domain at pH 4.0. (A) Cartoon diagram showing the *Mtb*-DHBPS monomer with secondary structure elements labeled. The α-helices, β-strands and loops are shown in red, yellow and green respectively. The phosphate and zinc molecules are shown in ball-and-stick and sphere model, respectively. (B) Stereoview of the F_o-F_c electron density map covering sulphate and zinc atom contoured at 5.0 σ level. Residues marked in red are from the neighbouring subunit. The interactions are shown in dotted lines. (C) Superposition of *Mtb*-DHBPS monomers with sulphate (green) and zinc and sulphate complex (pink).

Fig. 6. Comparison of *Mtb*-DHBPS domain structures from pH 6.0 and pH 4.0. (A) Superposition of *Mtb*-DHBPS monomers from pH 6.0 (blue) and pH 4.0 (pink). (B) Stereo diagram showing the close view of conformational change of loops connecting β7 and α6 and β1 and β2. The extension of α6-helix is marked with an arrow mark. (C) Superposition of *Mtb*-DHBPS (green) monomer at pH 4.0 with DHBPS structures from *C. albicans* (pink), *M. jannaschii* (yellow) and *M. grisea* (magenta) showing three loops (Loop1, Loop2 and Loop3) in different orientations.

TABLE 1

Data collection and Refinement statistics for *Mtb*-DHBPS domain

Parameters	pH 6.0	pH 4.0	pH 4.0+Zn
Data collection statistics			
Wavelength (Å)	0.973	1.542	1.542
Resolution range (Å)	50.00-1.80	50.00-2.06	50.00-2.06
Last resolution shell	1.86-1.80	2.13-2.06	2.13-2.06
Space group	C2	$P6_1$	$P6_1$
Unit cell parameters (Å)	a=89.78 b=51.32 c=95.41 β=112.76°	a=b=66.09 c=88.19	a=b=65.44 c=87.74
Unique reflections	35705	13377	13031
Redundancy	5.9 (4.8)[a]	6.0 (5.1)	7.3 (5.0)
Overall <I>/<σ(I)>	20.0 (3.5)	33.9 (10.0)	48.7 (5.7)
Completeness (%)	96.4 (78.8)	98.8 (88.9)	98.7 (87.2)
R_{merge} (%)[b]	8.7 (36.3)	4.8 (17.9)	4.7 (29.3)
Mosaicity (°)	1.5	0.6	0.7
Refinement statistics			
Resolution range (Å)	43.99-1.80	34.93-2.06	34.69-2.06
Last resolution shell	1.85-1.80	2.12-2.06	2.12-2.06
Unique reflections	35669	13375	13031
Completeness (%)	96.0 (72.8)	99.5 (94.7)	99.2 (89.3)
R_{cryst} (%)[c]	18.5	18.8	19.2
R_{free} (%)[d]	23.3	23.8	23.6
r.m.s.d from ideality			
Bond length (Å)	0.014	0.015	0.013
Bond angle (^{o})	1.437	1.547	1.433
Ramachandran plot			
Most favoured (%)	94.9	97.4	95.6
Additionally allowed (%)	5.1	2.6	4.4
Generously allowed (%)	0.0	0.0	0.0
Average B-factor (Å^2)			
Protein	21.7	32.9	34.6
Solvent	32.3	41.3	41.4
PO_4 ion	26.4	----	----
SO_4 ion	----	59.9	89.2
Glycerol	47.3	----	----
Zinc	----	----	101.8
PDBID	3MIO	3MGZ	3MK5

[a]Values for the last shell are in parentheses

[b]$R_{merge} = \Sigma_{hkl}\Sigma_i|I_i(hkl)-\langle I(hkl)\rangle|/\Sigma_{hkl}\,\Sigma_i\, I_i(hkl)$, where I(*hkl*) is the intensity of reflection *hkl*

[c]$R_{cryst} = \Sigma_{hkl}\,||F_{obs}|-|F_{calc}||/\Sigma|F_{obs}|$

[d]R_{free} is the cross validation R-factor computed for the test set of 5% of unique reflections not included in the refinement.

Figure 1

Click here to download high resolution image

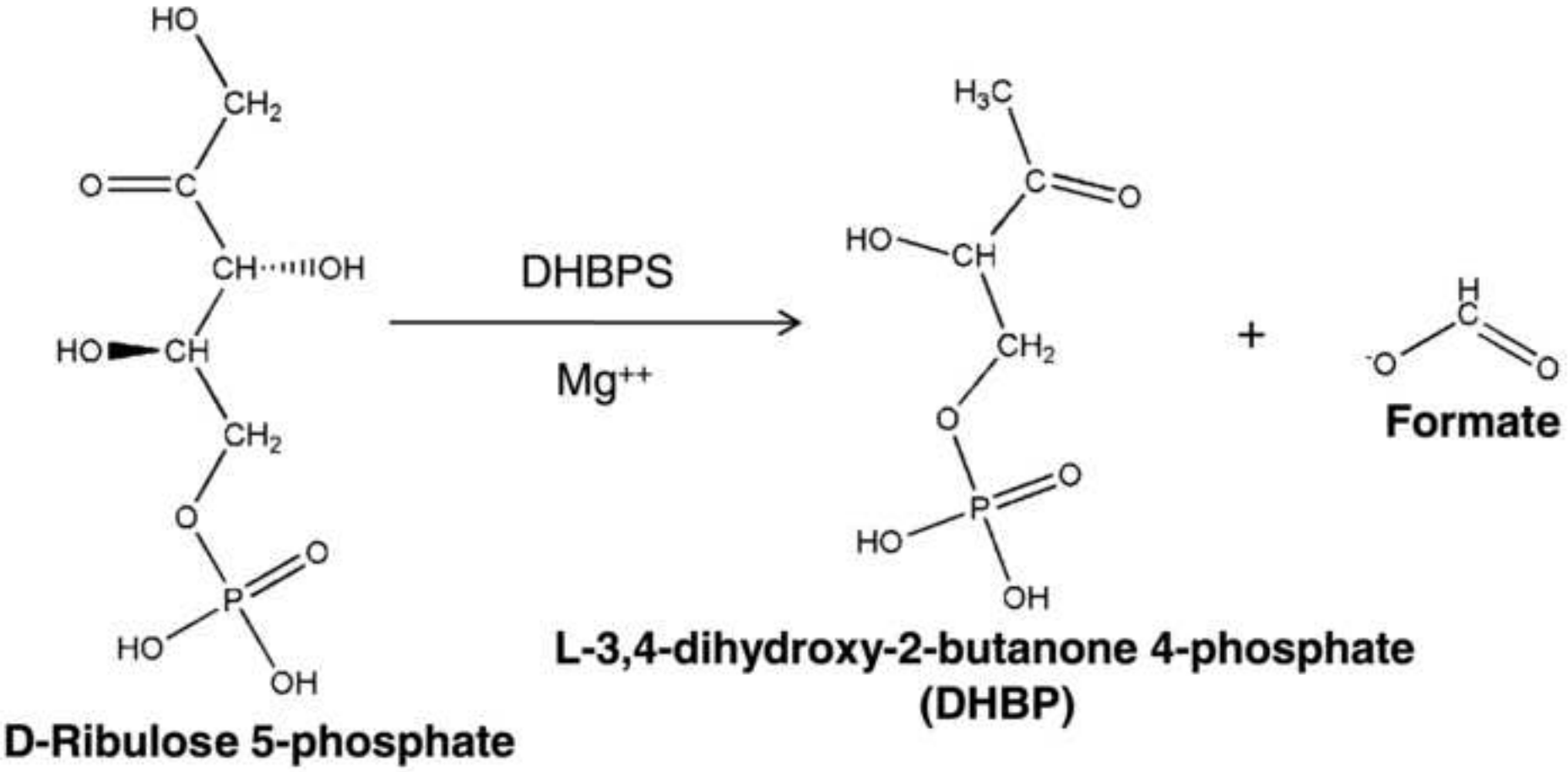

Figure 2

Click here to download high resolution image

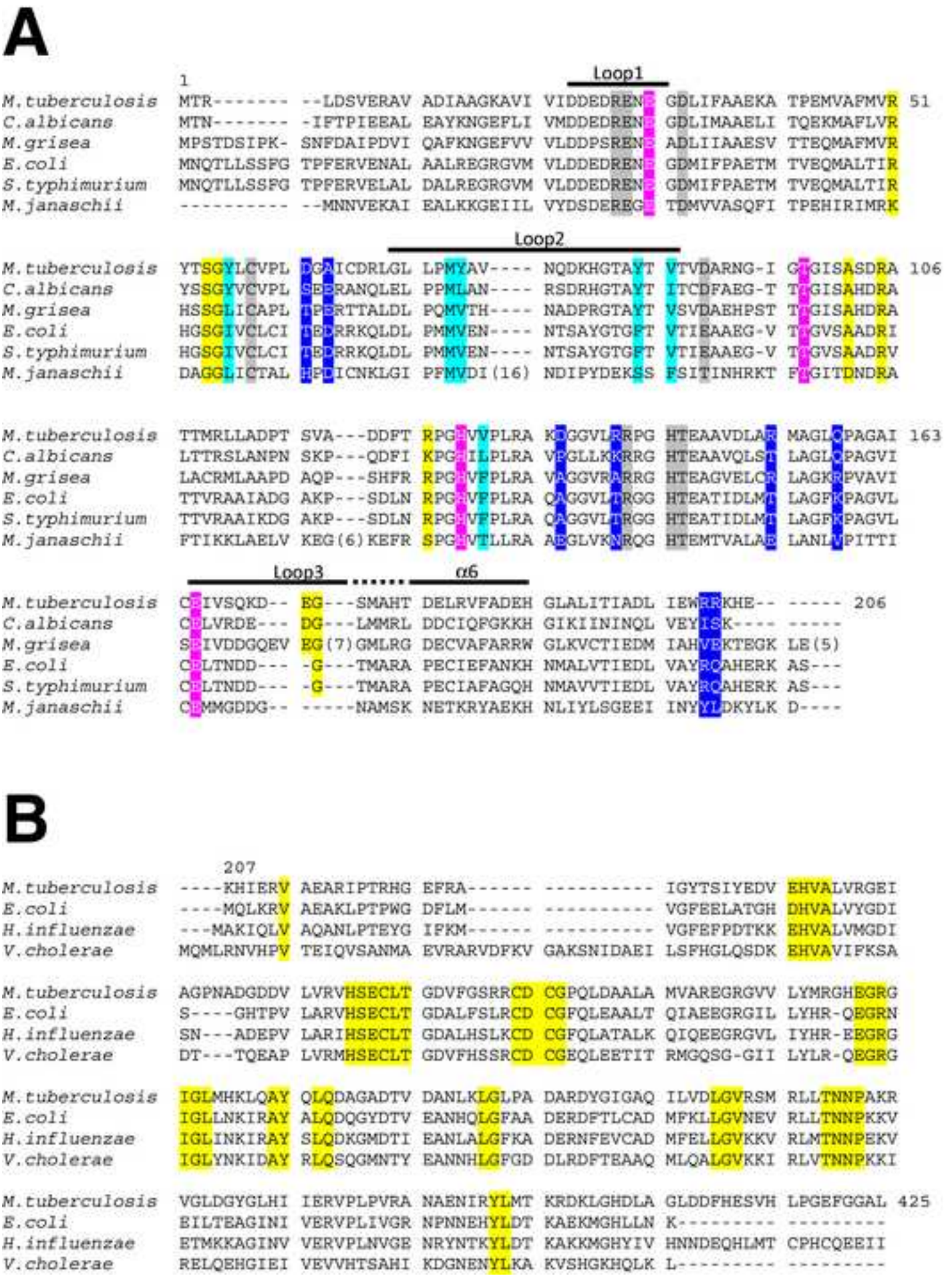

Figure 3

Click here to download high resolution image

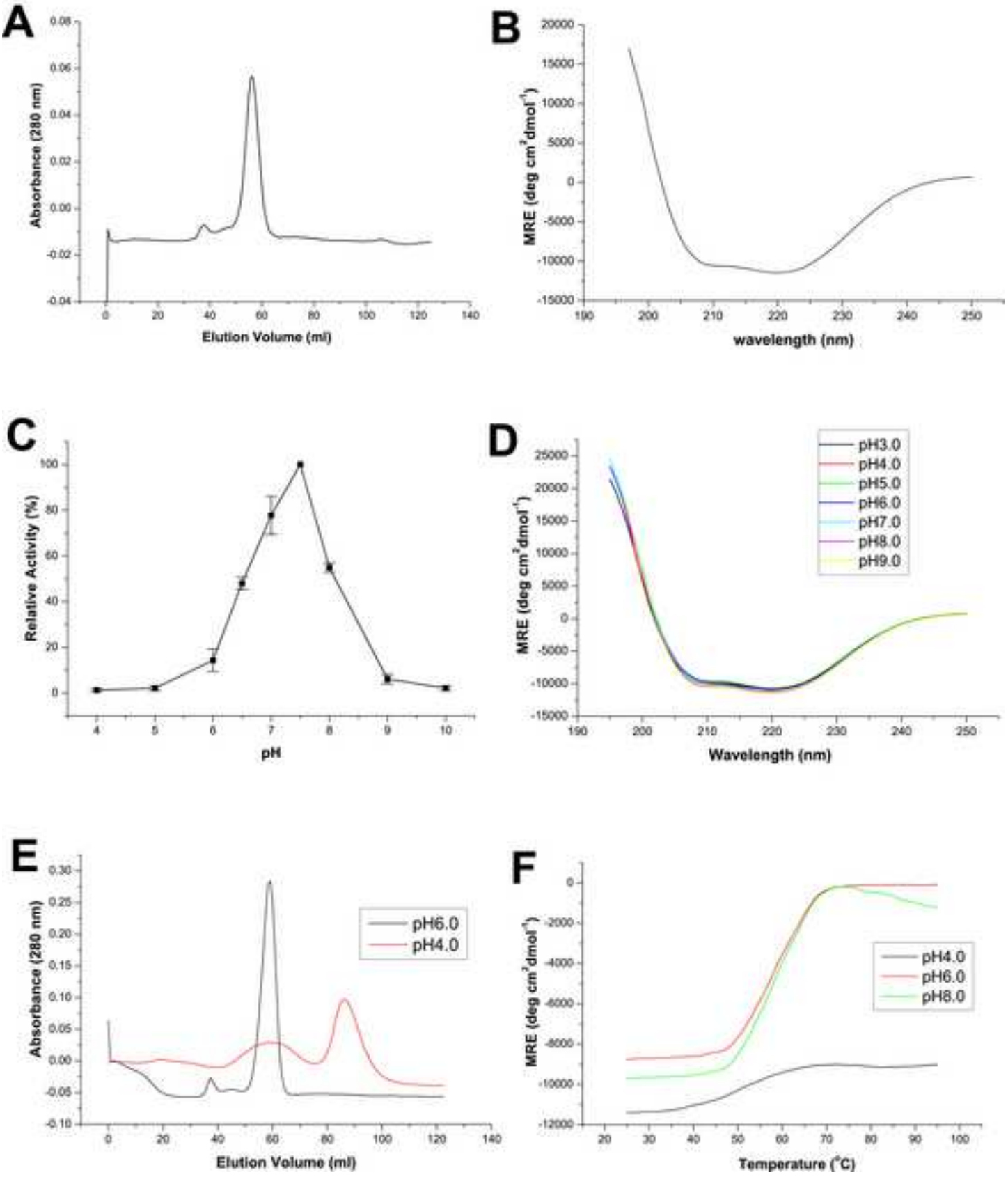

Figure 4

Click here to download high resolution image

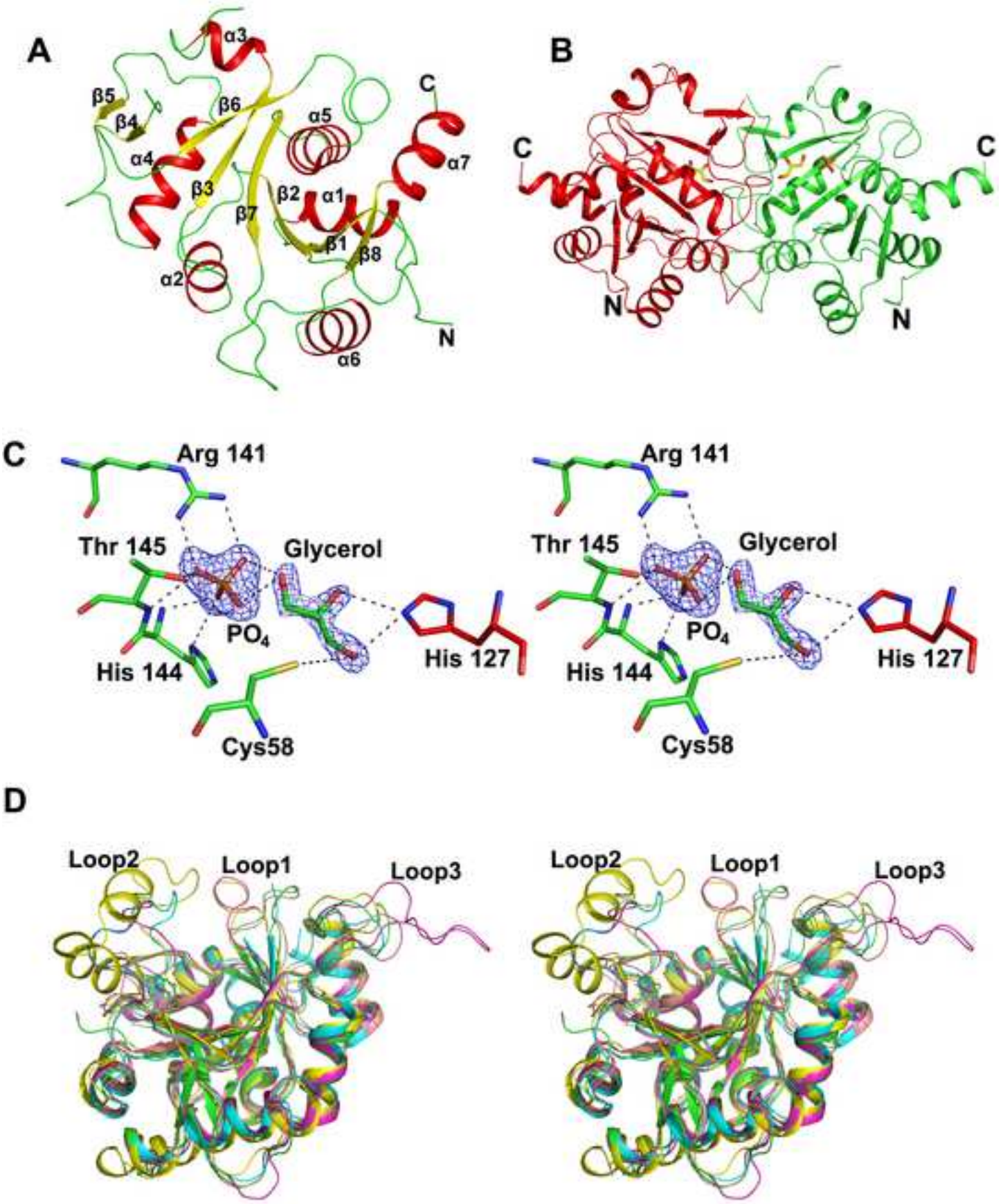

Figure 5

Click here to download high resolution image

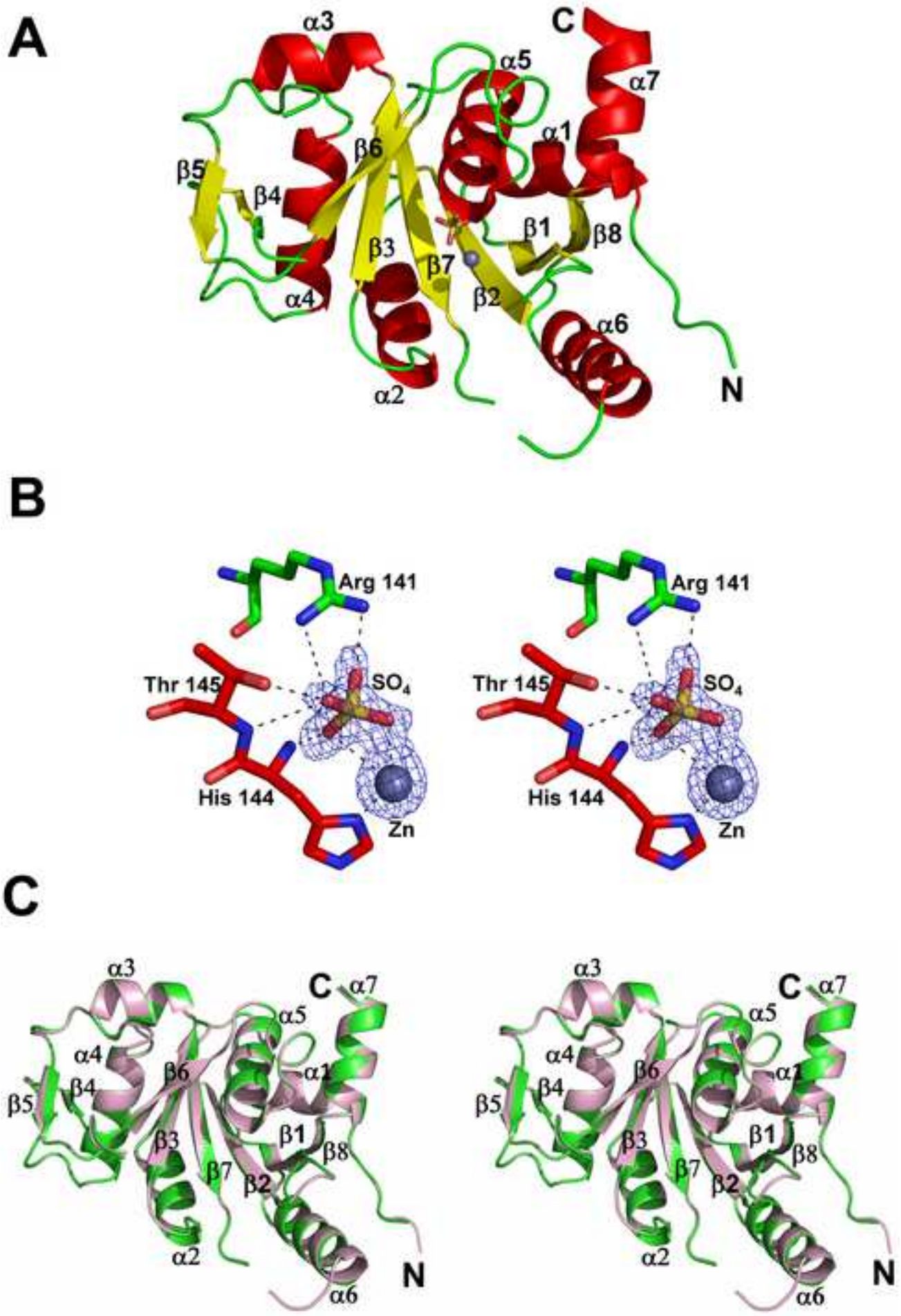

Figure 6

Click here to download high resolution image